Article

Journal of the Brazilian Chemical Society

https://dx.doi.org/10.21577/0103-5053.20240114

J. Braz. Chem. Soc. **2024**, *35*, 12, e-20240114, 1-12

Cobalt(II) Schiff-Base Complexes with Substituents of Varying Electron-Withdrawing Character: Synthesis, Characterization, DFT Calculations and Application as Electrocatalysts for Oxygen Reduction Reaction

Fagner S. Moura,[a,b] Everton T. da Silva,[c] Talis U. da Silva,[a] Rachel D. dos Santos,[a] Sérgio P. Machado,[a] Francisco M. S. Garrido,[,a] Marta E. Medeiros[*,a] and Annelise Casellato[a]*

[a]*Departamento de Química Inorgânica, Instituto de Química, Universidade Federal do Rio de Janeiro, 21941-909 Rio de Janeiro-RJ, Brazil*

[b]*Departamento de Química, Pontifícia Universidade Católica do Rio de Janeiro, 22453-900 Rio de Janeiro-RJ, Brazil*

[c]*Instituto Federal de Educação, Ciência e Tecnologia do Rio de Janeiro, Unidade Duque de Caxias, 25050-100 Duque de Caxias-RJ, Brazil*

Developing new non-noble metal electrocatalysts for oxygen reduction reaction (ORR) is an essential challenge in electrochemical device research. Among these, we highlight the metal Schiff-base complexes, which can be used as modified carbon paste electrodes (CPE). Herein, we present a facile one-pot method for preparing a new family of cobalt(II) complexes with Schiff-base ligands obtained from glycine and *para*-substituted aldehydes. Complexes were characterized by different techniques, and the effects of *para*-substituents on the electronic properties of the complexes were confirmed by ultraviolet-visible spectroscopy and cyclic voltammetry (CV). The CV was also used to evaluate the ORR behavior of metal complex-modified CPE in an alkaline medium. The three complex-modified CPE were found to be highly effective for ORR, and the electron-withdrawing character of *para*-substituent affects the electrochemical reactivity. Density functional theory (DFT) calculations were used to complement the study and correlate the electrochemical activity, the redox potentials, and the Hammett parameter (σ_p) with the singly occupied molecular orbital (SOMO) energy of the complexes. DFT data were also able to shed light on the likely ORR mechanism. In summary, electronic tuning of the ligand affects the electronic properties of the metal center and allows for systematic oxygen reduction-catalytic control.

Keywords: oxygen reduction reaction, Schiff-base, cobalt complexes, energy devices, Hammett parameters, DFT

Introduction

The demand for new energy-efficient and environmentally friendly technologies has led researchers to focus on the search for efficient and cost-effective electrocatalysts that can be used in electrochemical devices.[1-9] The oxygen reduction reaction (ORR, cathodic reaction) ranks among the essential half-reactions in various energy devices such as fuel cells and rechargeable metal-air batteries.[1,9,10] The ORR can be considered a limiting factor for the efficiency of these devices, mainly due to the use of high cost electrocatalysts (Pt or Pd), which are limited in availability and susceptible to poisoning.[1,5,7-11]

Coordination chemistry has been useful in developing new non-noble metal catalysts for electrochemical devices.[11-17] Many research groups have turned their attention to the development of different coordination compounds as ORR electrocatalysts, such as metalloporphyrins, metallophthalocyanines, metallocorroles, metal-organic frameworks (MOFs), and other types of metal complexes.[1,4,5,10,11,13,18] Among these, we highlight coordination compounds containing Schiff-bases ligands; these compounds are cheaper and easier to prepare compared to metalloporphyrins or metallophthalocyanines and can be used as modified graphite paste electrodes.[12,18-21]

*e-mail: chico@iq.ufrj.br; martam@iq.ufrj.br
Editor handled this article: Célia M. Ronconi (Associate)

Schiff-bases are considered privileged ligands because of their extremely flexible synthesis, as they can be easily prepared by condensation between amines and aldehydes or ketones.[13,19,20]

Schiff-base ligands coordinate many different metals and stabilize them in various oxidation states, allowing the use of Schiff-base metal complexes for various practical applications.[19,20] Several metals coordinated with Schiff-base ligands have been used to modify electrodes for application in ORR electrocatalysis, such as iron,[21-23] nickel,[12,24] copper,[11,18,25,26] and cobalt.[19,27,28] The great versatility of these compounds in terms of ligand structural modifications allows the modulation of their physical and chemical properties.[13,19-21] Unlike other coordination compound classes, studies on ORR mechanisms in metallic Schiff base complexes are rare.[11,26-29] Therefore, questions about the ORR mechanism for Schiff-base cobalt(II) complexes remain open.[15,16,29] For ORR in an alkaline medium, the adsorbed hydroxyl species may be essential to determine which mechanisms are most likely, for example, (*i*) outer sphere electron transfer (OSET) or (*ii*) inner sphere electron transfer (ISET).[29-31] In an alkaline medium, an essential characteristic of cobalt(II) Schiff-base complexes is that they can undergo ligand dissociation with the possibility of introducing OH^- or OH_2 into their coordination sphere.[32-34] This fact may be relevant in the ORR mechanism for this type of Co^{2+} complexes.[16]

Mixing graphite with mineral oils forms a heterogeneous mixture known as carbon paste (Figure S1a in the Supplementary Information (SI) section).[35] Carbon paste is an attractive material for electrode preparation (CPE). Its advantages include low cost, easy surface renewal, wide potential window, low background current, and ohmic resistance.[35] In recent years, numerous works have used chemically modified carbon paste electrodes with various transition metal complexes (Figure S1 in the SI section) or transition metal oxides; these electrodes are being widely used in various electrochemical applications.[12,18,35-40]

In the first part of the present work, we report the synthesis and structural characterization of a new family of cobalt(II) complexes with Schiff-base ligands obtained from glycine and *para*-substituted aldehydes. Each of the three ligands used (Lx = L1, L2, or L3) shows a different electron-withdrawing group (L1= H, L2 = Cl, and L3 = NO_2). The cobalt(II) complexes $[Co(Lx)_2]$ were characterized by Fourier transform infrared (FTIR) and UV-Vis spectroscopic methods, cyclic voltammetry, and powder X-ray diffraction. The complexes with the L2 = Cl and L3 = NO_2 are novel. In the second part of this paper, the coordination complexes were used to prepare complex-modified carbon paste electrodes (CoLx-CPE). These electrodes were tested for ORR in an alkaline medium. The effect of the substituent in the ORR was evaluated using the cyclic voltammetry technique. Density functional theory (DFT) calculations complement the study and correlate the ORR redox potentials with the singly occupied molecular orbital (SOMO) energy of the complexes. We also used DFT calculations to shed light on the probable mechanism of ORR in the alkaline medium for this type of complex.

Experimental

General procedure for the synthesis of the complexes $[Co(Lx)_2]$

All reagents and products used were purchased commercially without any previous treatment. The cobalt(II) complexes ($[Co(L1)_2]$, $[Co(L2)_2]$ and, $[Co(L3)_2]$) were synthesized *in situ* using a facile one-pot synthesis methodology reported previously, with modifications.[12] The Schiff-bases were prepared by the reaction of equimolar amounts of salicylaldehyde (0.61 g, 5 mmol, Sigma-Aldrich, Milwaukee, USA) for complex $[Co(L1)_2]$ 4-chlorosalicylaldehyde (0.78 g, 5 mmol, Sigma-Aldrich, Milwaukee, USA) for complex $[Co(L2)_2]$, and 4-nitrosalicylaldehyde (0.92 g, 5 mmol, Sigma-Aldrich, Milwaukee, USA) for complex $[Co(L3)_2]$), with glycine (0.38 g, 5 mmol, Sigma-Aldrich, Milwaukee, USA) in 100 mL of a methanolic solution of potassium hydroxide (0.28 g, 5 mmol, Sigma-Aldrich, Milwaukee, USA), resulting in a bright yellow solution which was kept under magnetic stirring for 2 h at room temperature. Then, $Co(OAc)_2{\cdot}4H_2O$ (1.25 g, 5 mmol, Vetec, Rio de Janeiro, Brazil) was dissolved in 30 mL of methanol (Sigma-Aldrich, Milwaukee, USA) and added gently to the reaction mixtures (ligands solutions), resulting in brownish solutions. The final solutions were left under magnetic stirring at room temperature for 2 h. After 3-6 days, dark brown microcrystalline materials were obtained with 75-90% yield. All the complexes are colored solids that are air-stable for an extended period but decompose at higher temperatures (> 150 ºC). The proposed structures of the complexes are shown in Scheme 1.

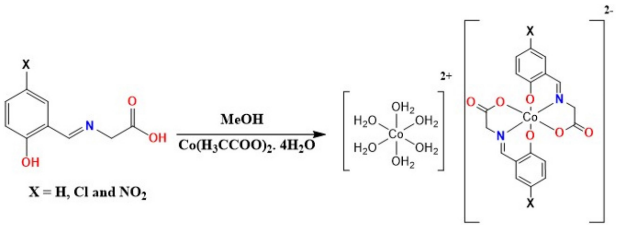

Scheme 1. Synthesis of cobalt(II) complexes (X = H (L1), Cl (L2), and NO_2 (L3)).

Preparation of the carbon paste electrode (CPE) and complex-modified electrodes (CoLx-CPE)

The graphite paste was prepared by mechanically mixing 0.02 g of powdered graphite with 20 μL of mineral oil to obtain a homogeneous paste (Figure S1a in the SI section). For the preparation of the carbon paste electrode (CPE), the graphite paste was placed into the bottom cavity at the end of a glass tube (working electrode), with a surface area of 7.07×10^{-2} cm^2, diameter of 3.00 mm, and depth of 1.00 mm, and electrical contact was made through a platinum disk (Figures S1b and S1c in the SI section). The three CoLx-CPE complex-modified electrodes (where Lx = L1, L2 or L3) were prepared using the same methodology as the CPE, but adding, respectively, one of the coordination compounds [Co(Lx)$_2$] (where L1 = H, L2 = Cl and L3 = NO$_2$) in the graphite paste, as described elsewhere.[12,18] The amount of each cobalt(II) complex ([Co(Lx)2]) in the CoLx-CPE complex-modified graphite pastes was 30% (m/m). In preparing the three CoLx-CPE modified electrodes, each complex-modified graphite paste was placed into the bottom cavity at the end of a glass tube of the working electrode (Figures S1b and S1c in the SI section).[12,18]

Characterization and electrochemical measurements

The powder X-ray diffraction pattern (PXRD) was collected using a Rigaku Ultima IV (185 mm) diffractometer (Rigaku Corporation, Japan) with Cu Kα radiation (Figures 1, and S2 and S3 in the SI section). The infrared analyses were performed using a NICOLET MAGNA-IR 760 spectrophotometer (Nicolet Corporation, USA) with a DGTS detector, 4 cm^{-1} resolution (Figures S4 to S6 in the SI section). The studies were done in the 4000 to 400 cm^{-1} (mid) region, using KBr (Merck, Rio de Janeiro, Brazil) disks. The electronic spectra in the ultraviolet-visible (UV-Vis) regions were obtained in an Agilent 8453 UV-Vis spectrophotometer (Agilent Technologies, USA). The analyses were performed in the 200-1100 nm region using spectroscopic methanol (Tedia, Fairfield, USA) solution at appropriate concentrations (Figures S7 to S11 in the SI section). The samples were analyzed in a quartz cuvette with a 1 cm optical path. A Metrohm AUTOLAB PGSTAT 128N potentiostat/galvanostat (Metrohm, Switzerland) was used to record the cyclic voltammetry (CV). The electrochemical characterization of the complexes by the cyclic voltammetry technique (Figures S12 to S14 in the SI section) was carried out using a three-electrode system: glassy carbon working electrode, saturated calomel reference electrode (SCE) and platinum counter electrode. The measurements were carried out at different scanning speeds, in the potential range suitable for each complex, under an N_2 atmosphere (White Martins, Rio de Janeiro, Brazil). A spectroscopic dimethyl sulfoxide (DMSO) solution (Sigma-Aldrich, Milwaukee, USA) of $TBAPF_6$ (0.05 mol L^{-1}, Sigma-Aldrich, Milwaukee, USA) was used as a supporting electrolyte.

A three-electrode system was used to study the electrochemical behavior of the metal complex-modified carbon paste electrodes (CoLx-CPE), in an alkaline medium. Platinum wire was used as a counter electrode, saturated calomel electrode (SCE), as a reference electrode, and the CPE or the complex-modified CPE as the working electrodes (Figures S1b and S1c in the SI section). The electrocatalytic activity of the CPE and of the complex-modified pastes towards the molecular oxygen reduction reaction was evaluated with a 0.1 mol L^{-1} NaOH (Merck, Rio de Janeiro, Brazil) solution as an electrolyte (Figures S15 to S17 in the SI section). The measurements were carried out in the range of –0.2 to –1.0 V or in the range of +1.0 to –1.0 V (Figures S15 to S17 in the SI section), with a sweep speed of 50 mV s^{-1}, in an inert atmosphere (N_2, White Martins, Rio de Janeiro, Brazil) and O_2 (White Martins, Rio de Janeiro, Brazil). Three consecutive cycles were performed for each analysis carried out in the range of –0.2 to –1.0 V.

Computational details

The density functional theory (DFT) calculations were performed using the B3LYP hybrid functional in Gaussian 09.[41-43] The Stuttgart-Dresden effective core potential (SDD) was used for the cobalt atom, and other atoms were treated with the 6-31+G(d) basis set.[44,45] Calculations were done in the gas phase and with a water solvent effect using the integral equation formalism polarized continuum model (IEF-PCM).[46] The binding energy was calculated using the equation $E_{binding} = E_{complex\text{-}OH} - (E_{complex} + E_{OH^-})$, where E is the electronic energy of each species.[47] Frequency calculations were performed to confirm that the structures were at an energetic minimum on the potential surface. The structure of the complex with $-NO_2$ presented an imaginary frequency and was therefore disregarded. The imaginary frequency indicates that the structure corresponds to a transition state, not a local energy minimum.

Results and Discussion

Powder X-ray diffraction (PXRD)

Figure 1 shows experimental and simulated PXRD patterns of complex [Co(L1)$_2$]. The experimental results

match very well with the theoretical patterns calculated with CIF files as input,[48] confirming the formation of the complex described by Han *et al*.[49] The absence of additional reflections proves the phase purity of the complex $[Co(L1)_2]$.

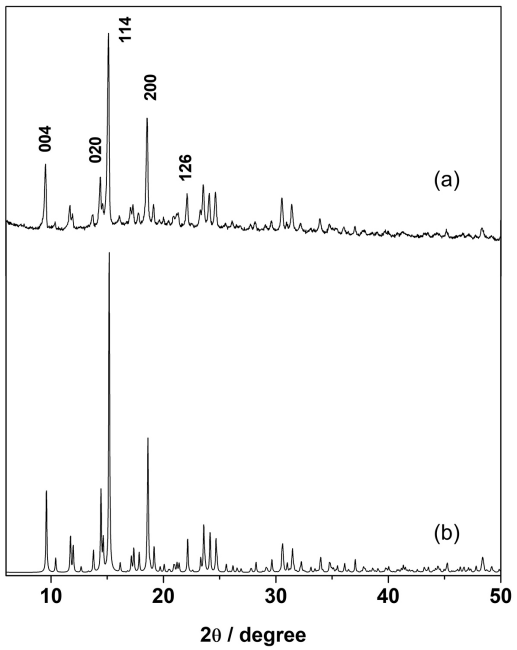

Figure 1. The PXRD spectrum of complex $[Co(L1)_2]$, (a) experimental results; (b) calculated using Cambridge Structural Database (CSD) under the code UGENUQ.[48,49]

For the two new complexes $[Co(L2)_2]$ and $[Co(L3)_2]$, the diffraction pattern reveals the crystalline nature of these complexes (Figures S2 and S3 in the SI section). X-ray powder data are especially useful for deducing accurate cell parameters without a single crystal. It is also possible to index the PXRD peaks with the same crystalline system as complex $[Co(L1)_2]$, an orthorhombic unit cell, showing that it is reasonable to consider that these complexes are isostructural. The cell parameters of the complexes are shown in Table 1. The indexing procedures used the ERACEL software,[50] considering the orthorhombic crystalline system. It is worth noting that complexes with similar Schiff-base ligands also form crystals with the orthorhombic crystalline system or octahedral metal geometry.[51-56]

Infrared spectra

In the absence of more powerful techniques such as single crystal X-rays, infrared spectra have proven to be a suitable technique to provide relevant information to elucidate the bonding mode of Schiff-base amino acid ligands.[57,58] The characteristic absorptions of the infrared spectra of the HLx Schiff-bases and $[Co(Lx)_2]$ complexes are listed in Table 2 (Figures S4 to S6 in the SI section). When analyzing the infrared spectra of all the complexes, it is possible to stand out bands related to the stretching vibration of the Co–O bonds between 537-543 cm^{-1} as well as the bands associated with the stretching vibration of the Co–N between 471-494 cm^{-1}, that are not observed in the spectra of free Schiff-base ligands.[59,60] When comparing the whole spectra of the free ligands with those of the metal complexes, it is possible to observe a shift of the bands to lower wavenumbers in the complexes, suggesting coordination to the metallic center, Table 2.[58-60] Upon comparison, the ν(C=N) of the azomethine stretching vibration was found in the free ligands between 1581-1627 cm^{-1}. This band is shifted to lower (16-28 cm^{-1}) wavenumbers in the complexes, indicating the involvement of the azomethine nitrogen in the coordination with the cobalt ion (Co–N).[59-61] All Schiff-base ligands showed a band in the region between 1374-1318 cm^{-1}, which can be attributed to the ν(C–O) of the phenolic group.[61] The shifting of these bands to lower wavenumbers values upon complexation indicates that the oxygen atoms of the phenolic groups are coordinated to the cobalt ion.[61] In the spectra of Schiff-bases, the two bands assignable to the asymmetric and symmetric stretching vibrations of the carboxylate groups are observed in the range of 1664-1650 cm^{-1} for $\nu(COO)_{asym}$ and between 1412-1344 cm^{-1} for $\nu(COO)_{sym}$. These bands are shifted to lower wavenumbers in the metal complexes spectra, showing that the oxygen atom of the carboxylate group is coordinated to the cobalt ion.[58-61]

The difference $\Delta\nu = [\nu(COO)_{asym}] - [\nu(COO)_{sym}]$ is a valuable characteristic tool to determine the coordination mode of the carboxylate group.[57,58,62] The difference in values of the band shift for the $[Co(Lx)_2]$ complexes was > 200 cm^{-1}, indicating that the carboxylate groups on the ligands are coordinated to the metal ion in a monodentate

Table 1. Cell parameters of the cobalt(II) complexes

Dimensions of unit cell	Literature data[49]	This work[a] $[Co(L1)_2]$	This work[a] $[Co(L2)_2]$	This work[a] $[Co(L3)_2]$
a / Å	9.560(4)	9.56	9.63	9.69
b / Å	12.253(5)	12.23	12.05	12.18
c / Å	36.854(15)	36.82	36.72	36.72
Alfa / degree	90.0	90.0	90.0	90.0
Beta / degree	90.0	90.0	90.0	90.0
Gamma / degree	90.0	90.0	90.0	90.0
Volume / $Å^3$	4317	4302	4261	4330

[a]Values calculated using the ERACEL software,[50] considering the orthorhombic crystalline system.

Table 2. Characteristic absorptions in the infrared spectra of the free ligands and their cobalt(II) complexes

	Absorption / cm^{-1}					
Compound	H_2L1	$[Co(L1)_2]$	H_2L2	$[Co(L2)_2]$	H_2L3	$[Co(L3)_2]$
$\nu(COO)_{asym}$	1650	1624	1664	1623	1659	1620
$\nu(COO)_{sym}$	1412	1370	1406	1314	1344	1315
$\Delta\nu$	–	254	–	309	–	305
ν(C=N)	1618	1600	1616	1588	1627	1581
ν(C=C)	1480	1450	1502	1451	1488	1444
$\nu(CO)_{phenol}$	1332	1303	1335	1311	1337	1319
ν(–CN)	1126	1081	1172	1134	1173	1107
ν(Co–O)	–	537	–	544	–	543
ν(Co–N)	–	471	–	494	–	474

mode.[58,62] The difference ($\Delta\nu$) value for similar cobalt Schiff-bases complexes reported in the literature are between 200-300 cm^{-1}.[59,60] Therefore, the infrared results are consistent with the formation of cobalt(II) complex with the two new Schiff-base ligands (L2 and L3), and these complexes show the exact structure figures of $[Co(L1)_2]$ complex, already described in the literature.[49]

Electronic spectra

In the electronic spectra of the complexes (Table 3), the most intense bands were observed in the high energy region around 270 and 380 nm, related to the $\pi \rightarrow \pi^*$ transitions of the aromatic ring and the azomethine group, respectively, besides ligand to metal charge transfer (LMCT) transition, which is characteristic of complexes with Schiff-based ligands (Figures S7 to S11 in the SI section).[49,63,64]

In the low energy region, it was possible to observe three low-intensity bands related to the d-d transition around 510, 690, and 960 nm, related to the ($\nu1$) $^4T_{1g} \rightarrow {}^4T_{1g}$ (P), ($\nu2$) $^4T_{1g} \rightarrow {}^4A_{2g}$ and ($\nu3$) $^4T_{1g} \rightarrow {}^4T_{2g}$ transitions, respectively.[18,49,63-65] These three transitions are consistent with an octahedral geometry for the two new cobalt complexes ($Co(L2)_2$ and $Co(L3)_2$).[49,63-65]

The study of the electronic spectra of cobalt(II) complexes indicates that the $–NO_2$ substituted ligand in $[Co(L3)_2]$ is weaker than the –H and –Cl ligands (in $[Co(L1)_2]$ and $[Co(L2)_2]$, respectively), this is due to the electroreceptor effect that the $–NO_2$ group has by reducing the electronic density available in the phenolic oxygen (coordinating atom) allowing the d orbitals of the metal ion to become less split, confirming the strong influence of the substituent on the electronic transitions.[66]

The λ_{max} for the complexes can show a relation to the Hammett parameter (σ_p) due to the influence of the substituents –H (L1), –Cl (L2), and $–NO_2$ (L3). The correlation between the energies (E) and the Hammett parameter (σ_p) and the bands around 380, 690, and 960 nm showed a *quasi*-linear behavior, as observed in Table 4 and Figure 2.[67] For $[Co(L3)_2]$, the bands were shifted to longer wavelengths, indicating that their orbitals are less distorted than those of the $[Co(L1)_2]$ and $[Co(L2)_2]$ complexes. The bathochromic effect is more pronounced in $[Co(L3)_2]$ because the $–NO_2$ group has a strong electron-withdrawing inductive effect, suggesting that the d orbitals of this complex are more stabilized than those of $[Co(L1)_2]$ and $[Co(L2)_2]$ complexes. It is possible to suggest a decrease in the availability of oxygen electrons in the phenol group since the $–NO_2$ group battles with the charge of the phenol group and the metal ion. This effect causes a minor split between the d orbitals, causing a smaller splitting of the d-orbitals (Δ) than when replaced with H or Cl (with lower withdrawal power), decreasing the energy of the transitions.[66]

Based on the electronic spectra of the complexes and on the *quasi*-linear correlation between the transition energies *versus* the Hammett parameter (σ_p), it is assumed that the three complexes are isostructural and have the same structure as the complex $[Co(L1)_2]$, published by in the literature.[49,63-67]

Electrochemical characterization

The electrochemical properties of these complexes were investigated by CV in DMSO with 0.05 mol L^{-1}

Table 3. Values of λ_{max}, the molar absorptivity coefficients ε, and attribution for the different absorptions ($\nu1$, $\nu2$, and $\nu3$) presented by the complexes in methanolic solution

$[Co(L1)_2]$		$[Co(L2)_2]$		$[Co(L3)_2]$		Attribution
λ_{max} / nm	ε / (L mol^{-1} cm^{-1})	λ_{max} / nm	ε / (L mol^{-1} cm^{-1})	λ_{max} / nm	ε / (L mol^{-1} cm^{-1})	
273	8372	275	15,382	272	30,361	($\pi \rightarrow \pi^*$)
376	2762	383	3,931	393	7,957	LMCT
510	442	565	309	513	810	$^4T_{1g} \rightarrow {}^4T_{1g}$ ($\nu1$)
687	174	690	128	695	161	$^4T_{1g} \rightarrow {}^4A_{2g}$ ($\nu2$)
967	86	975	47	982	12	$^4T_{1g} \rightarrow {}^4T_{2g}$ ($\nu3$)

LMCT: ligand to metal charge transfer.

Table 4. Energies of the transitions (ν1, ν2, and ν3) observed in the electronic spectra and the Hammett parameter (σ_p) for the substituted complexes studied ([Co(L1)$_2$], [Co(L2)$_2$] and [Co(L3)$_2$])

Transition	Energy / J		
	[Co(L1)$_2$]	[Co(L2)$_2$]	[Co(L3)$_2$]
ν1 (J)	5.28×10^{-19}	5.18×10^{-19}	5.05×10^{-19}
ν2 (J)	2.89×10^{-19}	2.87×10^{-19}	2.85×10^{-19}
ν3 (J)	2.05×10^{-19}	2.03×10^{-19}	2.02×10^{-19}
σ_p	0.00	0.22	0.78

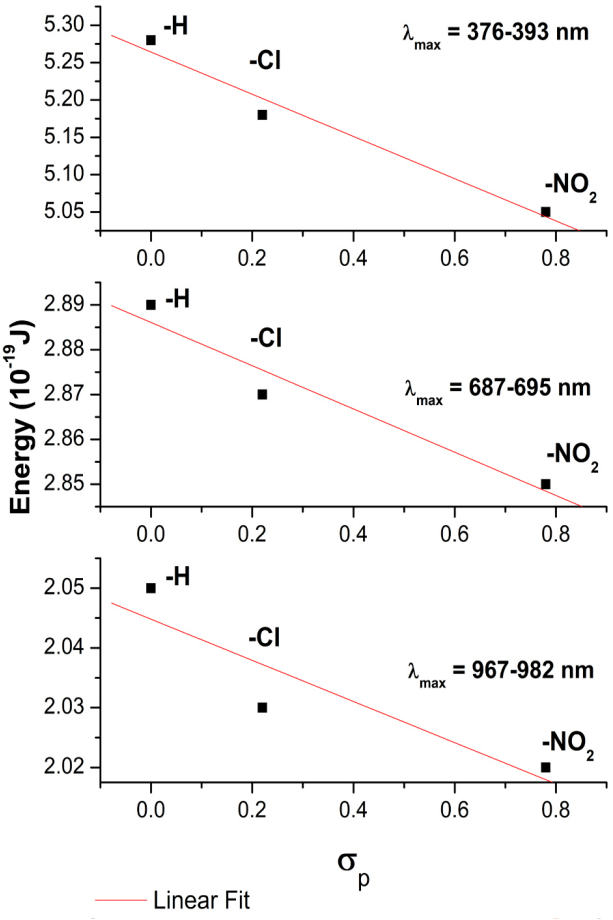

Figure 2. Comparison between the energy of electronic transitions and Hammett parameter (σ_p), in spectroscopic methanol.

$TBAPF_6$ as the supporting electrolyte at a glassy carbon working electrode under N_2 atmosphere at 25 °C (Figures S12 to S14 in the SI section). As can be observed in Figure 3, the influence of the ligands on the anodic peak of their corresponding cobalt complexes is a clear sign of the effect of the substituent groups on the donor capacity of the phenol rings. Indeed, a linear correlation between the Hammett parameters and the anodic peak can be observed in Figure 3.[68-71] Therefore, this linear correlation is other robust evidence that the three complexes are isostructural.[67-72]

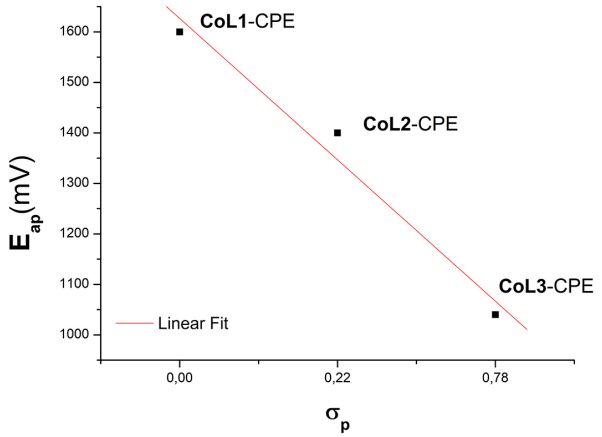

Figure 3. Correlation between the Hammett parameter (σ_p) and the anodic potential (E_{ap}) of the complexes.

According to the literature,[69-71] this anodic peak can be attributed to the oxidation of Co^{II} to Co^{III}. The values of these anodic peaks are related to the SOMO energies of complex and can be used to evaluate the relative energy of these orbitals.[14,31] The energy values of the highest occupied molecular orbital (HOMO) or SOMO orbitals are used to predict the behavior of electrocatalysts in the ORR, with a volcano-shape curve behavior being observed for metal phthalocyanines and metal porphyrins with different substituents.[14,15,31,73-76]

In the atmosphere of N_2 (Figures S12 to S14 in the SI section), the analysis of voltammograms obtained in DMSO solution also showed poorly defined redox peaks in the range −0.2 to −0.25 V, which could be attributed to the reduction of Co^{II} to Co^{I}.[69,70]

Electrochemical behavior of the cobalt(II) complex-modified electrodes (CoLx-CPE) in the presence of O_2

To study the electrochemical behavior of the complex-modified electrodes (CoLx-CPE: CoL1-CPE, CoL2-CPE, and CoL3-CPE, prepared by the addition of complexes [Co(L1)$_2$], [Co(L2)$_2$] or [Co(L3)$_2$], respectively) cyclic voltammetry was performed in an alkaline medium and a potential range of +1.0 to −1.0 V, under N_2 and O_2 atmospheres (Figures S15 to S17 in the SI section). In the tests carried out in the presence of O_2, an increase in the reduction current was observed for the complex-modified electrodes (CoLx-CPE) compared to the unmodified CPE (Figures S15 to S17 in the SI section).

To evaluate the capacity of the [Co(L1)$_2$], [Co(L2)$_2$] and [Co(L3)$_2$] complexes to catalyze the ORR, cyclic voltammetry was performed in a potential range of −0.2 to −1.0 V, under O_2 atmospheres (Figure 4), using the complex-modified electrodes (CoLx-CPE): CoL1-CPE, CoL2-CPE, and CoL3-CPE. For the unmodified CPE

electrode, the O_2 reduction peak is also observed, but this occurs at a more negative value (–0.64 V); see Figures S15 to S17 in the SI section. Therefore, the voltammograms of the three modified electrodes evaluated showed a cathodic peak that can be related to the reduction of molecular oxygen (Figure 4).[14,17,18,21-28]

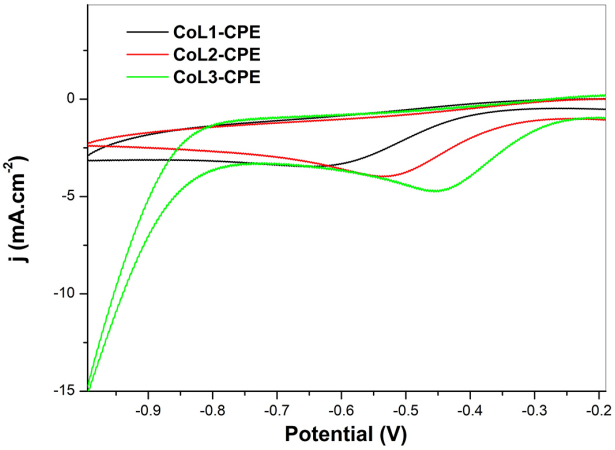

Figure 4. Cyclic voltammograms of CoL1-CPE, CoL2-CPE and CoL3-CPE in 0.1 mol L^{-1} NaOH solution saturated with O_2 gas, at scan rate 25 mV s^{-1} and saturated calomel electrode (SCE) as a reference electrode.

Comparing the electrocatalytic activity tests, Figure 4 shows a clear shift in the cathodic peaks. CoL1-CPE had the most negative potential (–0.60 V), and CoL3-CPE shifted to less negative values (–0.46 V), showing the least negative potential for the modified electrodes studied. A suggestion for the less negative potential observed in the CoL3-CPE voltammogram is that the $–NO_2$ group has a more substantial electron-withdrawing inductive effect; therefore, it applies a more considerable influence on the electronic structure of the cobalt(II) complex and, consequently, on the values of the reduction peaks.[72]

Hence, it is possible to relate the cathodic peak of the oxygen reduction reaction catalyzed by the complexes to the Hammett parameter (σ_p) in a nearly perfect linear correlation ($R^2 > 0.99$), as evidenced by Figure 5.

By analyzing the obtained results, the ORR is observed around the same potential as that for the reduction of Co^{II} to Co^{I} (around –0.50 V *vs*. SCE) in the alkaline medium, which was observed under an inert atmosphere (Figures S15 to S17 in the SI section). Therefore, the metallic center may be responsible for transferring the electrons that promotes the reduction of molecular oxygen.[18,73]

Therefore, the metallic center combined with different ligands promotes changes in the relative energies of the orbitals where electron transfers will take place. DFT calculations evaluated this hypothesis.

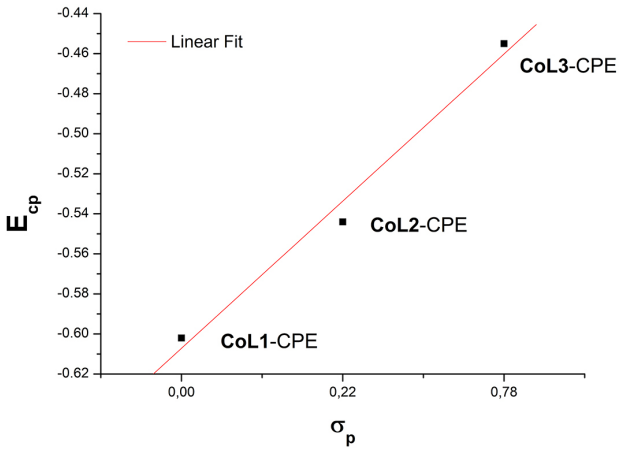

Figure 5. Linear relationship between the Hammett parameter (σ_p) and the cathodic potential (E_{cp}) in O_2 atmosphere of CoL1-CPE, CoL2-CPE, and CoL3-CPE, in O_2 atmosphere.

Theoretical studies

The optimized structures of the complex anions were obtained for doublet and quartet spin states. The calculated energy values in the –H and –Cl complexes indicated that the quartet state has lower energy than the doublet within the 12.1 to 13.3 kcal mol^{-1} range.

The positions and numbers of the selected atoms of $[Co(L1)_2]$ (the complex with –H) are presented in Figure 6. The calculated bond lengths and angles agreed with the experimental results (Table 5). The crystalline structure obtained by Han *et al.*[49] was used for comparison. This structure is available in the Cambridge Structural Database (CSD) under the code UGENUQ.[48]

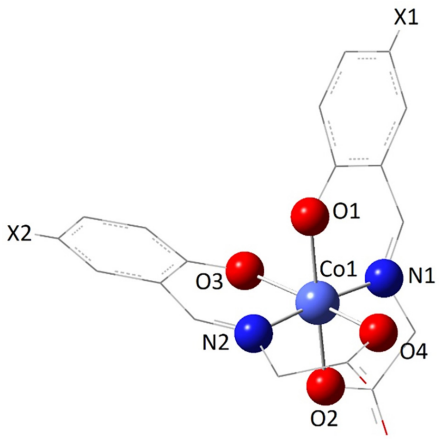

Figure 6. General structure of the investigated complexes (X1 and X2 = *para*-substituents).

The frontier molecular orbital analysis showed that the energy of these orbitals (lowest unoccupied molecular orbital (LUMO) and SOMO) and $gap_{L\text{-}S}$ (LUMO-SOMO energy gap) decreased in the order –H > –Cl > $–NO_2$ (Table 6 and Figure 7). The gap of the complexes can be

Table 5. Structural parameters of the complex $[Co(L1)_2]$

	$[Co(L1)_2]$				
	Doublet		Quartet		Exp.[40]
	Gas	Water	Gas	Water	
	Bond length / Å				
Co1–O1	2.01	1.98	2.13	2.10	1.87
Co1–N1	1.90	1.91	2.09	2.11	1.89
Co1–O2	2.03	2.01	2.14	2.16	1.93
Co1–O3	2.20	2.19	2.13	2.10	1.87
Co1–N2	1.92	1.95	2.09	2.11	1.89
Co1–O4	2.21	2.27	2.14	2.15	1.91
C–X1[a]	1.09	1.08	1.09	1.08	0.93
C–X2[a]	1.09	1.08	1.09	1.08	0.93
	Angle / degree				
O1–Co1–O2	175.6	177.1	165.9	164.1	179.4
O3–Co1–O4	170.4	168.9	165.9	164.1	178.5
N1–Co1–N2	175.4	175.8	173.3	178.8	173.5
O1–Co1–N1	92.3	93.0	86.5	86.3	94.7
O1–Co1–N2	91.1	90.0	94.1	94.1	89.5
O1–Co1–O3	84.5	88.7	87.8	94.6	90.4
O1–Co1–O4	91.2	89.3	92.1	90.8	90.1
O2–Co1–N1	84.5	84.2	79.5	78.4	85.5
O2–Co1–N2	92.2	92.8	100.0	101.1	90.3
O2–Co1–O3	92.6	92.3	92.0	90.9	89.0
O2–Co1–O4	92.1	90.2	91.4	87.9	90.5

[a]X1 = X2 = H.

Table 6. The energies of frontier molecular orbital (LUMO, SOMO, and $gap_{L\text{-}S}$) of the of studied complexes

	Co^{2+} complex					
	–H	–Cl	$–NO_2$	–H	–Cl	$–NO_2$
MO	Doublet (gas) / eV			Doublet (water) / eV		
LUMO	4.53	3.93	2.25	–1.08	–1.33	–
SOMO	1.64	1.17	0.34	–4.36	–4.52	–
$Gap_{L\text{-}S}$	2.89	2.77	1.91	3.28	3.19	–
	Quartet (gas) / eV			Quartet (water) / eV		
LUMO	4.56	3.98	–	–1.04	–1.28	–1.98
SOMO	0.80	0.35	–	–4.94	–5.14	–5.56
SOMO-1	0.78	0.26	–	–5.07	–5.25	–5.56
SOMO-2	0.68	0.24	–	–5.15	–5.32	–5.68
$Gap_{L\text{-}S}$	3.76	3.63	–	3.90	3.86	3.57

MO: molecular orbital; LUMO: lowest unoccupied molecular orbital; SOMO: singly occupied molecular orbital.

used to predict their kinetic stability; a more significant gap implies a higher kinetic stability.[14,73,77-79] Therefore, the order of the kinetic stability follows the same trend presented above: –H > –Cl > $–NO_2$. According to the literature,[14,29] the greater reactivity (lower energy gap) of the $[Co(L3)_2]$ complex must play a relevant role in the ORR.

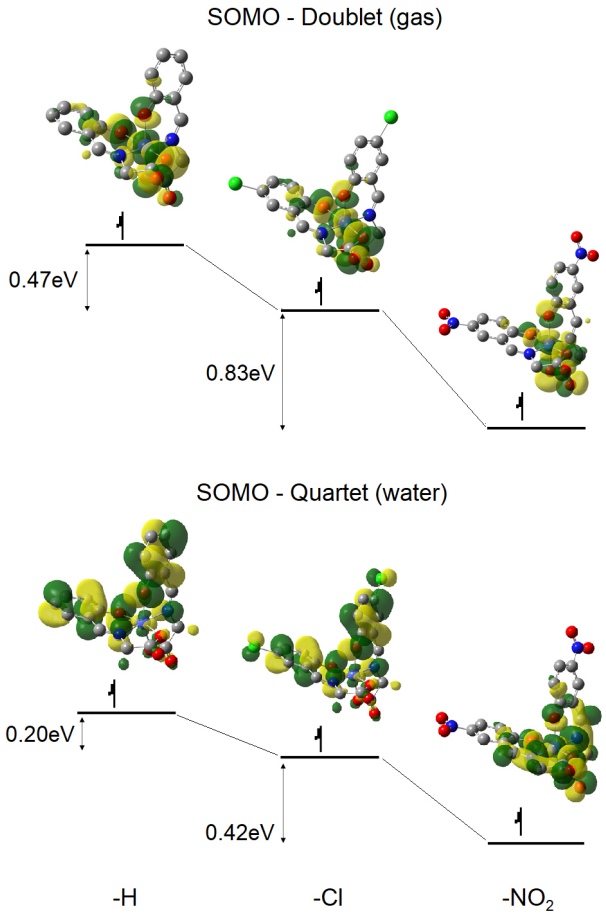

Figure 7. Comparison between the energies (eV) of the SOMO orbital in the complexes.

The energy of the SOMO orbital has an excellent correlation with the cathodic potential (E_{cp}) of the cobalt(II) complex-modified CPE (Figures 7 and 8). Also, the E_{SOMO} and the $gap_{L\text{-}S}$ showed a good correlation with the Hammett parameter (σ_p) and the anodic potential (E_{pa}) of the cobalt(II) complexes (Figures S18 and S19 in the SI section). The correlation of E_{SOMO} energy with the results of the anodic potential (E_{pa}) can be considered a strong indication that the DFT calculations adequately represent the studied cobalt(II) complexes.[14,31] Therefore, it can be considered that these cobalt(II) complexes are isostructural.

The graph of Figure 8 shows the same behavior as the graphs of the Hammett parameter *vs.* E_{SOMO} (Figure S18 in the SI section), which is a good indication of the effect of the substituent on the energy of the complex's orbitals and the impact of this electronic change on the reactivity against the oxygen reduction reaction.[14,31] In summary, the more negative the SOMO energy of the cobalt(II) complex, the less negative the E_{cp} for ORR to occur. This correlation can be considered a strong indication that the SOMO orbitals of the cobalt(II)

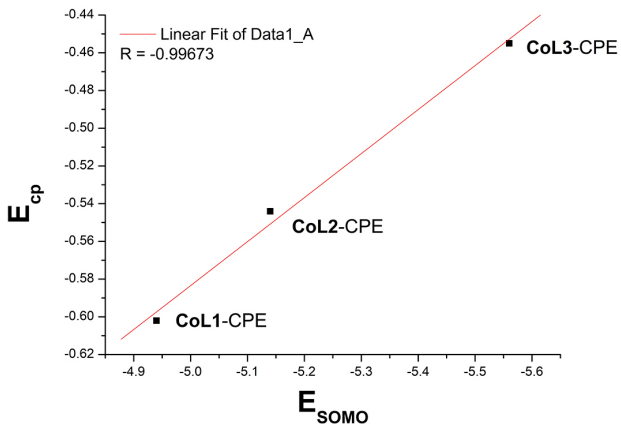

Figure 8. Linear relationship between the energy of the SOMO (quartet in water) and the cathodic potential (E_{cp}) of CoL1-CPE, CoL2-CPE, and CoL3-CPE, in O_2 atmosphere.

complexes have effective participation in the ORR process; similar behavior was observed for metalloporphyrins and metallophthalocyanine-based electrocatalysts.[4,14,31,73,75]

However, it is still necessary to better understand the mechanism of ORR in an alkaline medium in the metal Schiff-base complex-based electrocatalysts. In the mechanism of Xu *et al.*,[29] for cobalt porphyrin-based electrocatalyst, the complex with OH^- played an essential role in the catalytic action of the studied complexes in an alkaline medium. Therefore, the binding energy between the cobalt(II) Schiff-base complexes and OH^- were calculated to understand better the catalytic activity of these complexes (Table 7), considering the mechanisms described in the literature for ORR.[29,30]

Table 7. Binding energy ($E_{binding}$), for the reaction of the complex with OH^-

Complex	–H	–Cl	$–NO_2$
$E_{binding}$ / (kcal mol^{-1})	–238,4	–259,1	–60,8

The coordination of the OH^- resulted in breaking the bond of the O(phenolate) with the metal, and similar experimental results were observed for cobalt(II) complexes in an alkaline medium.[32-34] The O(phenolate) group was stabilized through a hydrogen bond with the OH^- (Figure 9). The $–NO_2$ complex had the lowest $E_{binding}$ with the OH^-, which can be understood by the electron density withdrawing nature of the nitro group. The Mulliken charge of the O(phenolate) (–0.68) in this complex had the least negative value, indicating a lower strength of the hydrogen bond (Figure 9).

This lower interaction should influence the catalytic action of the complex ($[Co(L3)_2]$) because, in the mechanism proposed by Xu *et al.*,[29] the complex loses the OH^-. Therefore, the greater ease in releasing OH^- predicted for this complex allows the catalytic cycle to continue

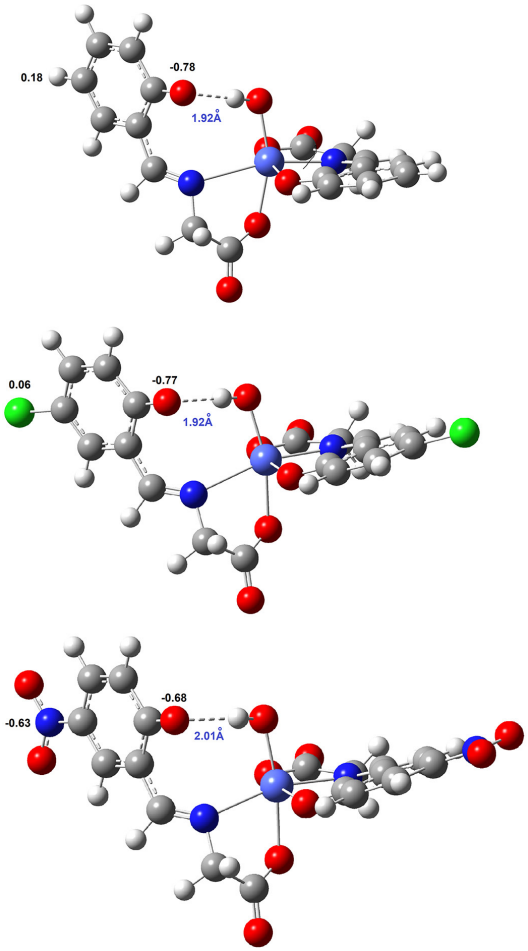

Figure 9. Complexes with OH^-. The Mulliken charges and hydrogen bond are shown.

forming the final species.[29] However, further studies are needed to determine the mechanism of this process in detail.

Based on the DFT calculations and the complex-modified electrodes (CoLx-CPE), we can suggest that the ORR process would be described in a simplified way by one of the following equations:[16,29,31,75]

4-electron reduction:

$$O_2 + 2H_2O + 4[Co^{I}(Lx)_2OH]^{4-} \rightarrow 8OH^- + 4[Co^{II}(Lx)_2]^{2-} \quad (1)$$

2-electron reduction:

$$O_2 + H_2O + 2[Co^{I}(Lx)_2OH]^{4-} \rightarrow HO_2^- + 3OH^- + 2[Co^{II}(Lx)_2]^{2-} \quad (2)$$

Conclusions

A family of complexes with ligands differing only in one aromatic ring substituent was obtained in the same experimental conditions. The experimental results of cobalt(II) complex ($Co(Lx)_2$) and complex-modified electrodes (CoLx-CPE) studies showed that the substituent

groups' effects affected the complexes' spectral and redox properties. In particular, the electrosensitive nature of the $–NO_2$ group facilitated the reduction of O_2, compared to –H and –Cl substituents. It was possible to correlate the cathodic peak of the oxygen reduction reaction catalyzed by the complexes-modified electrodes to the Hammett parameter (σ_p) in a linear correlation. DFT calculations showed a linear correlation between the energy of the SOMO orbital and the experimental parameters of the complexes, such as redox potentials and the Hammett parameter. The binding energy showed that the complex with the $–NO_2$ substituent has less interaction with $OH^–$, which may explain the order of the complexes in the ORR catalysis. In summary, DFT data provided information on the effect of complex/ligand structure on catalytic activity trends. DFT results also shed light on the likely mechanism of ORR in an alkaline medium for these cobalt(II) complexes.

Supplementary Information

Supplementary information includes XRPD, infrared and UV-Vis spectra, cyclic voltammograms, and other information about the cobalt(II) complexes, and they are available free of charge at http://jbcs.sbq.org.br as PDF file.

Acknowledgments

This work was supported by the Coordenação de Aperfeiçoamento de Pessoal de Nível Superior, Brasil (CAPES) (Funding Code 001; PhD Scholarship to TU da Silva). The authors also thank Fundação de Amparo à Pesquisa do Estado do Rio de Janeiro (FAPERJ) (Scholarship E-26/010.210.513/2019).

Author Contributions

Fagner S. Moura was responsible for data curation, formal analysis, investigation, and visualization; Everton T. da Silva was responsible for theoretical calculations, data curation, formal analysis, software, visualization, and writing-review and editing; Talis U. da Silva was responsible for theoretical calculations, data curation, formal analysis, software, and writing-review and editing; Rachel D. dos Santos was responsible for data curation, formal analysis, and investigation; Sérgio de P. Machado was responsible for the conceptualization, formal analysis, software, funding acquisition, and writing-review and editing; Marta E. Medeiros was responsible for the conceptualization, formal analysis, funding acquisition, and writing-review and editing; Francisco M. S. Garrido and Annelise Casellato were responsible for the conceptualization, formal analysis, funding acquisition, project administration, methodology, writing original draft, review and editing.

References

1. Chen, K.; Liu, K.; An, P.; Li, H.; Lin, Y.; Hu, J.; Jia, C.; Fu, J.; Li, H.; Liu, H.; Lin, Z.; Li, W.; Li, J.; Lu, Y. R.; Chan, T. S.; Zhang, N.; Liu, M.; *Nat. Commun*. **2020**, *11*, 4173. [Crossref]
2. Wang, Y.; Su, H.; He, Y.; Li, L.; Zhu, S.; Shen, H.; Xie, P.; Fu, X.; Zhou, G.; Feng, C.; Zhao, D.; Xiao, F.; Zhu, X.; Zeng, Y.; Shao, M.; Chen, S.; Wu, G.; Zeng, J.; Wang, C.; *Chem. Rev.* **2020**, *120*, 12217. [Crossref]
3. Yasin, G.; Ibrahim, S.; Ajmal, S.; Ibraheem, S.; Ali, S.; Nadda, A. K.; Zhang, G.; Kaur, J.; Maiyalagan, T.; Gupta, R. K.; Kumar, A.; *Coord. Chem. Rev.* **2022**, *469*, 214669. [Crossref]
4. Venegas, R.; Zúñiga, C.; Zagal, J. H.; Toro-Labbé, A.; Marco, J. F.; Menéndez, N.; Muñoz-Becerra, K.; Recio, F. J.; *ChemElectroChem* **2022**, *9*, e202200115. [Crossref]
5. Li, Z.; Gao, R.; Feng, M.; Deng, Y. P.; Xiao, D.; Zheng, Y.; Zhao, Z.; Luo, D.; Liu, Y.; Zhang, Z.; Wang, D.; Li, Q.; Li, H.; Wang, X.; Chen, Z.; *Adv. Energy Mater*. **2021**, *11*, 2003291. [Crossref]
6. Shah, R.; Ali, S.; Raziq, F.; Ali, S.; Ismail, P. M.; Shah, S.; Iqbal, R.; Wu, X.; He, W.; Zu, X.; Zada, A.; Adnan; Mabood, F.; Vinu, A.; Jhung, S. H.; Yi, J.; Qiao, L.; *Coord. Chem. Rev.* **2023**, *477*, 214968. [Crossref]
7. Bhoyate, S. D.; Kim, J.; de Souza, F. M.; Lin, J.; Lee, E.; Kumar, A.; Gupta, R. K.; *Coord. Chem. Rev.* **2023**, *474*, 214854. [Crossref]
8. Cruz-Navarro, J. A.; Mendoza-Huizar, L. H.; Salazar-Pereda, V.; Cobos-Murcia, J. Á.; Colorado-Peralta, R.; Álvarez-Romero, G. A.; *Inorg. Chim. Acta* **2021**, *520*, 120293. [Crossref]
9. Shin, D.; Bhandari, S.; Tesch, M. F.; Bonke, S. A.; Jaouen, F.; Chabbra, S.; Pratsch, C.; Schnegg, A.; Mechler, A. K.; *J. Energy Chem.* **2022**, *65*, 433. [Crossref]
10. Zhao, Y. M.; Yu, G. Q.; Wang, F. F.; Wei, P. J.; Liu, J. G.; *Chem. - Eur. J.* **2019**, *25*, 3726. [Crossref]
11. Muñoz-Becerra, K.; Zagal, J. H.; Venegas, R.; Recio, F. J.; *Curr. Opin. Electrochem.* **2022**, *35*, 101035. [Crossref]
12. dos Santos, R. D.; dos Santos, S. F. F.; Moura, F. S.; Maia, P. J. S.; da Fonseca, B. T.; Santos, R. H. A.; Medeiros, M. E.; Garrido, F. M. S.; Casellato, A.; *Transition Met. Chem.* **2017**, *42*, 301. [Crossref]
13. Freire, C.; Nunes, M.; Pereira, C.; Fernandes, D. M.; Peixoto, A. F.; Rocha, M.; *Coord. Chem. Rev.* **2019**, *394*, 104. [Crossref]
14. Zagal, J. H.; Griveau, S.; Silva, J. F.; Nyokong, T.; Bedioui, F.; *Coord. Chem. Rev.* **2010**, *254*, 2755. [Crossref]
15. Zúñiga Loyola, C.; Tasca, F.; *Curr. Opin. Electrochem.* **2023**, *40*, 101316. [Crossref]
16. Orellana, W.; Zuñiga, C.; Gatica, A.; Ureta-Zanartu, M. S.; Zagal, J. H.; Tasca, F.; *ACS Catal*. **2022**, *12*, 12786. [Crossref]
17. Yuan, S.; Peng, J.; Zhang, Y.; Zheng, D. J.; Bagi, S.; Wang, T.; Román-Leshkov, Y.; Shao-Horn, Y.; *ACS Catal.* **2022**, *12*, 7278. [Crossref]

18. Dionízio, T. P.; dos Santos, A. C.; da Silva, F. P.; da Silva Moura, F.; D'Elia, E.; dos Santos Garrido, F. M.; Medeiros, M. E.; Casellato, A.; *Electrocatalysis* **2021**, *12*, 137. [Crossref]
19. Kumar, M.; Singh, A. K.; Singh, A. K.; Yadav, R. K.; Singh, S.; Singh, A. P.; Chauhan, A.; *Coord. Chem. Rev.* **2023**, *488*, 215176. [Crossref]
20. Kanwal, A.; Parveen, B.; Ashraf, R.; Haider, N.; Ali, K. G.; *J. Coord. Chem.* **2022**, *75*, 2533. [Crossref]
21. Sen, P.; Akagunduz, D.; Aghdam, A. S.; Cebeci, F. Ç.; Nyokong, T.; Catal, T.; *J. Inorg. Organomet. Polym. Mater.* **2020**, *30*, 1110. [Crossref]
22. Velázquez-Palenzuela, A.; Zhang, L.; Wang, L.; Cabot, P. L.; Brillas, E.; Tsay, K.; Zhang, J.; *Electrochim. Acta* **2011**, *56*, 4744. [Crossref]
23. Rigsby, M. L.; J. Wasylenko, D.; Pegis, M. L.; Mayer, J. M.; *J. Am. Chem. Soc.* **2015**, *137*, 4296. [Crossref]
24. Wang, Y.; Shi, R.; Shang, L.; Waterhouse, G. I. N.; Zhao, J.; Zhang, Q.; Gu, L.; Zhang, T.; *Angew. Chem., Int. Ed.* **2020**, *59*, 13057. [Crossref]
25. Ma, Z.; Chu, Y.; Fu, C.; Du, H.; Huang, X.; Zhao, J.; *Catalysts* **2018**, *8*, 156. [Crossref]
26. Paul, A.; Silva, T. A. R.; Soliman, M. M. A.; Karačić, J.; Šljukić, B.; Alegria, E. C. B. A.; Khan, R. A.; Guedes da Silva, M. F. C.; Pombeiro, A. J. L.; *Int. J. Hydrogen Energy* **2022**, *47*, 23175. [Crossref]
27. Bai, L.; Li, M.; Guan, J.; *ChemistrySelect* **2018**, *3*, 581. [Crossref]
28. Feng, X.; Xu, Z.; Zhao, J.; Hansen, H. A.; Deng, Q.; *Int. J. Hydrogen Energy* **2022**, *47*, 27000. [Crossref]
29. Xu, Q.; Zhao, L.; Yuan, R.; Chen, Y.; Xue, Z.; Zhang, J.; Qiu, X.; Qu, J.; *Colloids Surf., A* **2021**, *629*, 127435. [Crossref]
30. Ramaswamy, N.; Mukerjee, S.; *J. Phys. Chem. C* **2011**, *115*, 18015. [Crossref]
31. Zúñiga-Loyola, C.; Ureta-Zanartu, M. S.; Tasca, F.; *J. Chem. Educ.* **2024**, *101*, 344. [Crossref]
32. Woźniczka, M.; Sutradhar, M.; Pombeiro, A. J. L.; Świątek, M.; Pająk, M.; Gądek-Sobczyńska, J.; Chmiela, M.; Gonciarz, W.; Pasternak, B.; Kufelnicki, A.; *Molecules* **2020**, *25*, 3462. [Crossref]
33. Woźniczka, M.; Sutradhar, M.; Chmiela, M.; Gonciarz, W.; Pająk, M.; *J. Inorg. Biochem.* **2023**, *249*, 112389. [Crossref]
34. Woźniczka, M.; Świątek, M.; Sutradhar, M.; Gądek-Sobczyńska, J.; Chmiela, M.; Gonciarz, W.; Pasternak, B.; Pająk, M.; *Comput. Struct. Biotechnol. J.* **2023**, *21*, 1312. [Crossref]
35. Turunc, E.; Gumus, I.; Arslan, H.; *Mater. Chem. Phys.* **2020**, *243*, 122597. [Crossref]
36. Shamsipur, M.; Najafi, M.; Hosseini, M. R. M.; Sharghi, H.; *Electroanalysis* **2007**, *19*, 1661. [Crossref]
37. Wang, X.; Zhao, H.; Lin, H.; Liu, G.; Fang, J.; Chen, B.; *Electroanalysis* **2008**, *20*, 1055. [Crossref]
38. Ourari, A.; Ketfi, B.; Malha, S. I. R.; Amine, A.; *J. Electroanal. Chem.* **2017**, *797*, 31. [Crossref]
39. Giarola, J. F.; Borges, K. B.; Tarley, C. R. T.; de Oliveira, F. M.; Ribeiro, E. S.; Pereira, A. C.; *Arabian J. Chem.* **2017**, *10*, 430. [Crossref]
40. Garrido, F. M. S.; Medeiros, R. F.; de Nogueira, N. O. B.; Peres, R. C. D.; Ribeiro, E. S.; Medeiros, M. E.; *Rev. Matéria* **2013**, *18*, 1294. [Crossref]
41. Becke, A. D.; *J. Chem. Phys.* **1993**, *98*, 5648. [Crossref]
42. Lee, C.; Yang, W.; Parr, R. G.; *Phys. Rev. B* **1988**, *37*, 785. [Crossref]
43. Frisch, M. J.; Trucks, G. W.; Schlegel, H. B.; Scuseria, G. E.; Robb, M. A.; Cheeseman, J. R.; Scalmani, G.; Barone, V.; Mennucci, B.; Petersson, G. A.; Nakatsuji, H.; Caricato, M.; Li, X.; Hratchian, H. P.; Izmaylov, A. F.; Bloino, J.; Zheng, G.; Sonnenberg, J. L.; Hada, M.; Ehara, M.; Toyota, K.; Fukuda, R.; Hasegawa, J.; Ishida, M.; Nakajima, T.; Honda, Y.; Kitao, O.; Nakai, H.; Vreven, T.; Montgomery Jr., J. A.; Peralta, J. E.; Ogliaro, F.; Bearpark, M.; Heyd, J. J.; Brothers, E.; Kudin, K. N.; Staroverov, V. N.; Kobayashi, R.; Normand, J.; Raghavachari, K.; Rendell, A.; Burant, J. C.; Iyengar, S. S.; Tomasi, J.; Cossi, M.; Rega, N.; Millam, N. J.; Klene, M.; Knox, J. E.; Cross, J. B.; Bakken, V.; Adamo, C.; Jaramillo, J.; Gomperts, R.; Stratmann, R. E.; Yazyev, O.; Austin, A. J.; Cammi, R.; Pomelli, C.; Ochterski, J. W.; Martin, R. L.; Morokuma, K.; Zakrzewski, V. G.; Voth, G. A.; Salvador, P.; Dannenberg, J. J.; Dapprich, S.; Daniels, A. D.; Farkas, Ö.; Foresman, J. B.; Ortiz, J. V.; Cioslowski, J.; Fox, D. J.; *Gaussian 09*, Revision, Gaussian, Inc.: Wallingford CT, 2009.
44. Bergner, A.; Dolg, M.; Küchle, W.; Stoll, H.; Preuß, H.; *Mol. Phys.* **1993**, *80*, 1431. [Crossref]
45. Dolg, M.; Wedig, U.; Stoll, H.; Preuss, H.; *J. Chem. Phys.* **1987**, *86*, 866. [Crossref]
46. Souza, M. L.; Castellano, E. E.; Telser, J.; Franco, D. W.; *Inorg. Chem.* **2015**, *54*, 2067. [Crossref]
47. Mallya, A. N.; Panda, S.; *Comput. Theor. Chem.* **2021**, *1202*, 113288. [Crossref]
48. CCDC, https://www.ccdc.cam.ac.uk/structures/Search?Ccdcid=UGENUQ&DatabaseToSearch=Published, accessed in June 2024.
49. Han, J.; Xing, Y. H.; Bai, F. Y.; Zhang, X. J.; Zeng, X. Q.; Ge, M. F.; *J. Coord. Chem.* **2009**, *62*, 2719. [Crossref]
50. Laugier, J.; Filhol, A.; Bail, A. L.; *ERACEL 1996*; University of Maine, France, 1996.
51. Liu, H. Y.; Guan, Q. H.; Tian, J.; Du, P.; Chen, H.; *Transition Met. Chem.* **2016**, *41*, 615. [Crossref]
52. Rodionova, L. I.; Smirnov, A. V.; Borisova, N. E.; Khrustalev, V. N.; Moiseeva, A. A.; Grünert, W.; *Inorg. Chim. Acta* **2012**, *392*, 221. [Crossref]
53. Ghosh, P.; Chowdhury, A. R.; Saha, S. K.; Ghosh, M.; Pal, M.; Murmu, N. C.; Banerjee, P.; *Inorg. Chim. Acta* **2015**, *429*, 99. [Crossref]

54. Muche, S.; Harms, K.; Burghaus, O.; Hołyńska, M.; *Polyhedron* **2018**, *144*, 66. [Crossref]
55. Naqi Ahamad, M.; Iman, K.; Raza, M. K.; Kumar, M.; Ansari, A.; Ahmad, M.; Shahid, M.; *Bioorg. Chem.* **2020**, *95*, 103561. [Crossref]
56. Mondal, S. S.; Jaiswal, N.; Bera, P. S.; Tiwari, R. K.; Behera, J. N.; Chanda, N.; Ghosal, S.; Saha, T. K.; *Appl. Organomet. Chem.* **2021**, *35*, e6026. [Crossref]
57. Nakamoto, K.; *Infrared and Raman Spectra of Inorganic and Coordination Compounds*, 4th ed.; John Wiley: New York, USA, 1986.
58. Hadjiivanov, K. I.; Panayotov, D. A.; Mihaylov, M. Y.; Ivanova, E. Z.; Chakarova, K. K.; Andonova, S. M.; Drenchev, N. L.; *Chem. Rev.* **2021**, *121*, 1286. [Crossref]
59. Mohamed, G. G.; Omar, M. M.; Hindy, A. M. M.; *Spectrochim. Acta, Part A* **2005**, *62*, 1140. [Crossref]
60. Singh, B. K.; Rajour, H. K.; Prakash, A.; *Spectrochim. Acta, Part A* **2012**, *94*, 143. [Crossref]
61. Abdel-Rahman, L. H.; El-Khatib, R. M.; Nassr, L. A. E.; Abu-Dief, A. M.; Ismael, M.; Seleem, A. A.; *Spectrochim. Acta, Part A* **2014**, *117*, 366. [Crossref]
62. Deacon, G. B.; Phillips, R.; *J. Coord. Chem. Rev.* **1980**, *33*, 227. [Crossref]
63. Abou-Melha, K. S.; Al-Hazmi, G. A.; Althagafi, I.; Alharbi, A.; Shaaban, F.; El-Metwaly, N. M.; El-Bindary, A. A.; El-Bindary, M. A.; *J. Mol. Liq.* **2021**, *334*, 116498. [Crossref]
64. Chandra, S.; Sharma, A. K.; *Spectrochim. Acta, Part A* **2009**, *72*, 851. [Crossref]
65. Lever, A. B. P.; *Inorganic Eletronic Espectroscopy*; Elsevier Science Publishers BV: Amsterdam, Netherlands, 1984.
66. Peralta, R. A.; Bortoluzzi, A. J.; de Souza, B.; Jovito, R.; Xavier, F. R.; Couto, R. A. A.; Casellato, A.; Nome, F.; Dick, A.; Gahan, L. R.; Schenk, G.; Hanson, G. R.; de Paula, F. C. S.; Pereira-Maia, E. C.; Machado, S. P.; Severino, P. C.; Pich, C.; Bortolotto, T.; Terenzi, H.; Castellano, E. E.; Neves, A.; Riley, M. J.; *Inorg. Chem.* **2010**, *49*, 11421. [Crossref]
67. Caro, C. A.; Cabello, G.; Landaeta, E.; Pérez, J.; González, M.; Zagal, J. H.; Lillo, L.; *J. Coord. Chem.* **2014**, *67*, 4114. [Crossref]
68. Arabahmadi, R.; *ChemistrySelect* **2019**, *4*, 4883. [Crossref]
69. Stojičkov, M.; Sturm, S.; Čobeljić, B.; Pevec, A.; Jevtović, M.; Scheitler, A.; Radanović, D.; Senft, L.; Turel, I.; Andjelković, K.; Miehlich, M.; Meyer, K.; Ivanović-Burmazović, I.; *Eur. J. Inorg. Chem.* **2020**, *2020*, 3347. [Crossref]
70. Kumar, S.; Hansda, A.; Chandra, A.; Kumar, A.; Kumar, M.; Sithambaresan, M.; Faizi, M. S. H.; Kumar, V.; John, R. P.; *Polyhedron* **2017**, *134*, 11. [Crossref]
71. Zúñiga, C.; Tasca, F.; Calderon, S.; Farías, D.; Recio, F. J.; Zagal, J. H.; *J. Electroanal. Chem.* **2016**, *765*, 22. [Crossref]
72. Zolezzi, S.; Spodine, E.; Decinti, A.; *Polyhedron* **2002**, *21*, 55. [Crossref]
73. Gulppi, M. A.; Recio, F. J.; Tasca, F.; Ochoa, G.; Silva, J. F.; Pavez, J.; Zagal, J. H.; *Electrochim. Acta* **2014**, *126*, 37. [Crossref]
74. Masa, J.; Schuhmann, W.; *Chem. - Eur. J.* **2013**, *19*, 9644. [Crossref]
75. Loyola, C. Z.; Abarca, G.; Ureta-Zañartu, S.; Aliaga, C.; Zagal, J. H.; Sougrati, M. T.; Jaouen, F.; Orellana, W.; Tasca, F.; *J. Mater. Chem. A* **2021**, *9*, 23802. [Crossref]
76. Riquelme, J.; Neira, K.; Marco, J. F.; Hermosilla, P.; Venegas, D.; Orellana, W.; Ponce, I.; Zagal, J. H.; Tasca, F.; *ECS Trans.* **2018**, *85*, 111. [Crossref]
77. Fu, Q.; He, T.; Guo, W.; Zhao, L.; Chai, Y.; Zhou, T.; Liu, Y.; Liu, C.; *J. Mol. Struct. THEOCHEM* **2009**, *906*, 6. [Crossref]
78. Jauris, I. M.; Fagan, S. B.; Adebayo, M. A.; Machado, F. M.; *Comput. Theor. Chem.* **2016**, *1076*, 42. [Crossref]
79. da Silva, E. T.; da Silva, T. U.; de Carvalho Pougy, K.; da Silveira, R. B.; da Silva, R. S.; Machado, S. P.; *Inorg. Chim. Acta* **2020**, *510*, 119724. [Crossref]

Submitted: February 1, 2024
Published online: June 27, 2024